A *Diaphanous*-related formin links Ras signaling directly to actin assembly in macropinocytosis and phagocytosis

Alexander Junemann[a], Vedrana Filić[b], Moritz Winterhoff[a], Benjamin Nordholz[a,1], Christof Litschko[a], Helena Schwellenbach[a], Till Stephan[a], Igor Weber[b], and Jan Faix[a,2]

[a]Institute for Biophysical Chemistry, Hannover Medical School, 30625 Hannover, Germany; and [b]Division of Molecular Biology, Ruđer Bošković Institute, 10000 Zagreb, Croatia

Edited by Thomas D. Pollard, Yale University, New Haven, CT, and approved October 5, 2016 (received for review July 6, 2016)

Phagocytosis and macropinocytosis are Ras-regulated and actin-driven processes that depend on the dynamic rearrangements of the plasma membrane that protrudes and internalizes extracellular material by cup-shaped structures. However, the regulatory mechanisms underlying actin assembly in large-scale endocytosis remain elusive. Here, we show that the *Diaphanous*-related formin G (ForG) from the professional phagocyte *Dictyostelium discoideum* localizes to endocytic cups. Biochemical analyses revealed that ForG is a rather weak nucleator but efficiently elongates actin filaments in the presence of profilin. Notably, genetic inactivation of ForG is associated with a strongly impaired endocytosis and a markedly diminished F-actin content at the base of the cups. By contrast, ablation of the Arp2/3 (actin-related protein-2/3) complex activator SCAR (suppressor of cAMP receptor) diminishes F-actin mainly at the cup rim, being consistent with its known localization. These data therefore suggest that ForG acts as an actin polymerase of Arp2/3-nucleated filaments to allow for efficient membrane expansion and engulfment of extracellular material. Finally, we show that ForG is directly regulated in large-scale endocytosis by RasB and RasG, which are highly related to the human proto-oncogene KRas.

Arp2/3 complex | formin | macropinocytosis | phagocytosis | Ras

The internalization of solid particles by phagocytosis and internalization of bulk fluid by macropinocytosis are closely related and evolutionary conserved clathrin-independent endocytic processes (1). In higher eukaryotes, as exemplified by neutrophils and macrophages, phagocytosis is a central part of the innate immune system responsible for the clearance of viral and bacterial pathogens (2), whereas the scavenging of nutrients and metabolites by macropinocytosis is considered increasingly important for tumor progression and cancer cell proliferation (3–5). Phagocytosis and macropinocytosis are actin-driven processes that entail rearrangements of the plasma membrane to engulf extracellular material, followed by delivery of the ingested material into lysosomes for extraction of nutrients (6). Morphologically, several stages can be distinguished, starting with the initiation of cup formation after detection of external cues via diverse G protein-coupled receptors, such as the Fc-γ and C3a receptors in mammalian cells (7), followed by membrane protrusion and the pursestring-like closure of the cup leading to the separation of the closed vesicle from the plasma membrane (6, 8).

The social amoeba *Dictyostelium discoideum* is a professional phagocyte that hunts bacteria by chemotaxis and ingests them by phagocytosis. Nevertheless, because cultivation on bacteria is difficult, most laboratories use axenic strains that can grow through uptake of liquid media by macropinocytosis (9). Recent work interestingly revealed that macropinocytosis in these strains is strongly improved due to a mutation in the *axeB* gene encoding the Ras GTPase-activating protein (RasGAP) neurofibromin 1 (NF1) (10). Due to its genetic tractability and ease of use, *D. discoideum* has become an attractive model organism that allows dissecting conserved mechanisms and signaling pathways of large-scale endocytosis (11). Comparable to mammalian cells, the initial steps of the underlying signaling cascades are quite well understood and are initiated by G protein-coupled folate receptor fAR1 activation upstream of heterotrimeric G proteins (12, 13). This step is followed by activation of small GTPases of the Ras family, which act as master regulators of diverse downstream signaling pathways, including target of rapamycin complex 2 (14) and class-I PI3-kinases (PI3Ks) (15), albeit *Dictyostelium* cells use ether-linked plasmanylinositides instead of phosphatidylinositides (16). PI3K1 and PI3K2 produce patches of phosphatidylinositol (3,4,5)-trisphosphate (PIP_3), which are linked to actin-dependent cup formation, whereas PI3K4 is required for the conversion of the cups into intracellular vesicles (15, 17). The latter process is associated with rapid disassembly of the F-actin coat (18), and, consistently, a number of F-actin depolymerization factors, including coronin, actin-interacting protein (Aip1), and cofilin, were shown to participate in cup maturation and disassembly (18–20). Moreover, force generation by myosins was shown to play an important role in amoeba as well as in mammalian cells (17, 21, 22). However, it still remains elusive how Ras and PIP_3 signaling are linked to actin assembly on the molecular level to drive extensive membrane deformations during cup formation.

Eukaryotic cells mainly use two types of actin assembly factors. The Arp2/3 complex is composed of seven subunits and operates downstream of SCAR/WAVE (Wiskott–Aldrich syndrome

Significance

Macropinocytosis and phagocytosis are two Ras-regulated, highly related processes of great physiological relevance collectively termed large-scale endocytosis. Both are actin-driven and entail engulfment of extracellular material by crown-like protrusions. Aside from the Arp2/3 complex, which serves as the main nucleator of branched actin filaments at the cup rim, the underlying mechanisms of actin assembly still remain elusive. Here, we analyzed the role of *Diaphanous*-related formin G (ForG) from *Dictyostelium* by biochemical, genetic, and imaging techniques. Our data demonstrate that this formin exhibits a rather weak nucleation activity and imply that ForG-mediated filament elongation synergizes with the Arp2/3 complex in actin assembly. Finally, we identify ForG as a Ras-regulated formin and show its significance for actin assembly in endocytic structures.

Author contributions: A.J., V.F., M.W., I.W., and J.F. designed research; A.J., V.F., M.W., B.N., C.L., H.S., T.S., I.W., and J.F. performed research; A.J., V.F., M.W., B.N., C.L., I.W., and J.F. analyzed data; and A.J. and J.F. wrote the paper.

The authors declare no conflict of interest.

This article is a PNAS Direct Submission.

Data deposition: The sequence reported in this paper has been deposited in the European Nucleotide Archive sequence data bank (accession no. LN901451).

[1]Deceased January 17, 2013.

[2]To whom correspondence should be addressed. Email: faix.jan@mh-hannover.de.

This article contains supporting information online at www.pnas.org/lookup/suppl/doi:10.1073/pnas.1611024113/-/DCSupplemental.

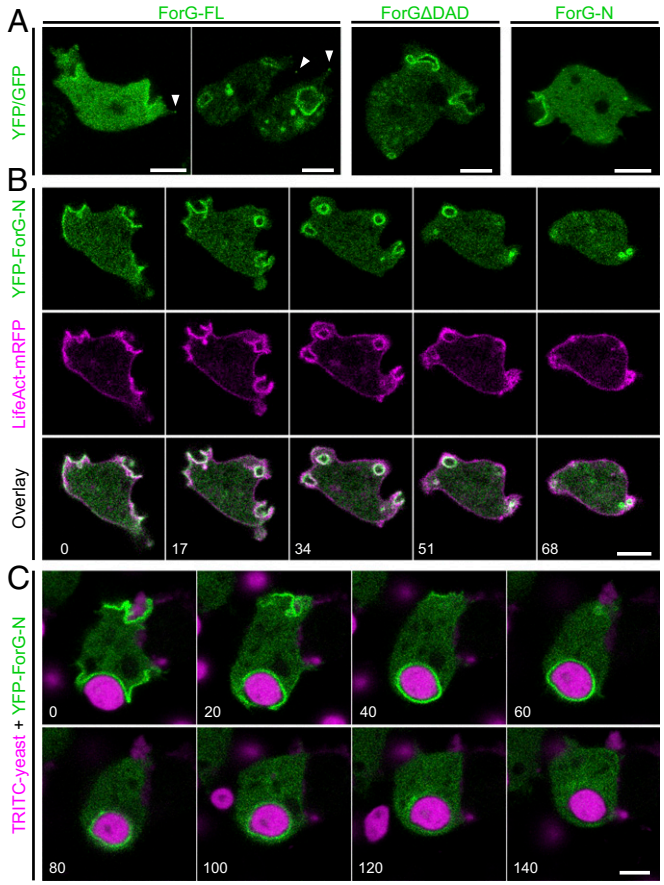

Fig. 1. ForG localizes to endocytic structures. (*A*) GFP-tagged ForG-FL, constitutively active ForGΔDAD (amino acids 1–1,040), and YFP–ForG-N (amino acids 1–423) ectopically expressed in vegetative *Dictyostelium* cells prominently localized to nascent macropinosomes. Faint enrichment at filopodia tips is indicated by white arrowheads. (*B*) Time-lapse imaging of cells coexpressing LifeAct-mRFP and YFP–ForG-N revealed that ForG localization is fairly distinct from cortical F-actin. (*Bottom*) Merged images illustrate striking colocalization of F-actin and ForG at macropinosomes. (*C*) YFP–ForG-N also accumulated at phagocytic cups throughout engulfment of the large TRITC-labeled yeast particles. Confocal sections are shown in *B* and *C*, and correspond to Movies S1 and S2. Time is given in seconds. (Scale bars: 5 μm.)

protein family verprolin-homologous protein) signaling to nucleate branches on the sides of existing mother filaments to generate a dense actin meshwork as illustrated by the actin architecture at the leading edge (23). Formins are dimeric multidomain proteins that nucleate and elongate linear actin filaments to form, for instance, filopodial bundles and cortical actin (24, 25). The proline-rich formin homology domain 1 (FH1) recruits profilin (PFN)–actin complexes for filament elongation, which is accomplished by the neighboring FH2 domain (24). Members of the subfamily of *Diaphanous*-related formins (DRFs) are tightly regulated. By virtue of additional regulatory sequences located in the N- and C-terminal regions, these proteins are intrinsically autoinhibited. Binding of Rho family GTPases to the N-terminal GTPase-binding domain (GBD) releases this autoinhibition and renders the protein active (24).

Here, we describe the role of *Diaphanous*-related formin G (ForG) from *D. discoideum* in large-scale endocytosis. We find ForG to be highly enriched in the cups of macropinosomes and phagosomes, and show that it is required for efficient uptake of fluid and solid particles. Our biochemical data further demonstrate that this formin exhibits rather weak nucleation activity in vitro, strongly suggesting that ForG mainly contributes to filament elongation during expansion and closure of the cups. Finally, our data reveal that ForG acts as a specific effector of active Ras-subfamily GTPases, demonstrating an unanticipated type of DRF regulation that, in turn, directly links Ras signaling to dynamic remodeling of the actin cytoskeleton in endocytosis.

Results

ForG Localizes to Nascent Macropinosomes and Phagosomes. Cups, sometimes referred to as crown-shaped membrane protrusions, are formed during large-scale uptake of nutrients in macropinocytosis and phagocytosis, and depend on dynamic F-actin polymerization (6). In *Dictyostelium* cells, the Arp2/3 activator SCAR/WAVE was previously found to localize exclusively to the rim of macropinocytic cups, whereas F-actin was highly enriched in the entire structure beneath the plasma membrane (8). We therefore asked whether formins, the second class of actin assembly factors present in *Dictyostelium*, may contribute to the generation of this specialized F-actin network and operate in large-scale endocytosis. Previously, we reported that the developmentally regulated formin C (ForC) of *Dictyostelium* cells localizes to endocytotic structures when ectopically expressed in vegetative cells (26). However, endogenous ForC only begins to accumulate after 6 h of development, at a time point when micropinocytosis has largely ceased (27), strongly indicating that ForC is not involved in macropinocytosis. Thus, we focused our attention on the closely related formin ForG, because previous real-time PCR data indicated continuous expression of this

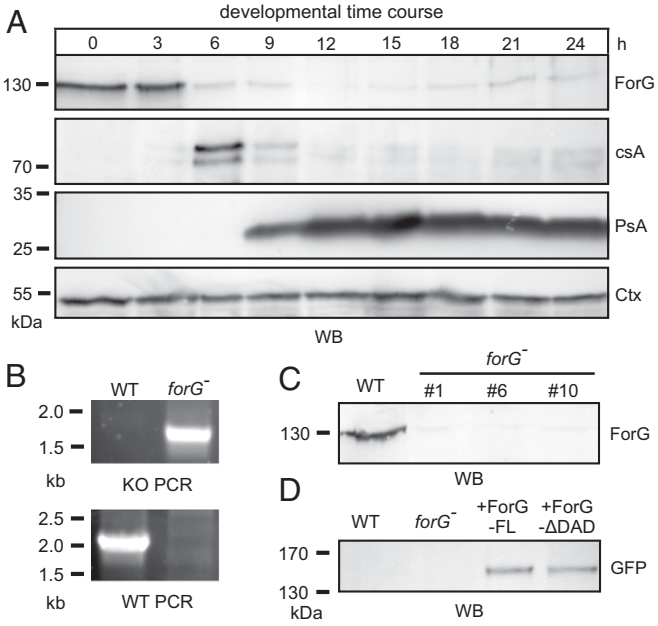

Fig. 2. ForG is expressed during vegetative growth and onset of development. (*A*) Expression of ForG during the development of the *D. discoideum* in the WT strain. Growth-phase cells (0 h) or developing cells (3–24 h) were harvested every 3 h and analyzed by SDS/PAGE and immunoblotting. ForG was maximally expressed during growth (0 h) and the onset of starvation (3 h). Thereafter, ForG protein levels sharply declined and remained at a low but constant level. The contact site A (csA) protein served as an early aggregation marker, and the prespore antigen A (PsA) specified the onset of differentiation. The constitutively expressed cortexillin (Ctx) was used as a loading control. (*B*) Inactivation of the *forG* gene was validated by two PCR assays to screen for disruption (KO) or the presence of the WT allele using specific primer pairs. (*C*) Absence of ForG in independent mutants was confirmed by Western blotting using anti-ForG antibodies. (*D*) Reconstitution of *forG*$^-$ cells with GFP-tagged ForG-FL and ForGΔDAD was confirmed by Western blotting (WB) using anti-GFP antibodies.

protein in growth-phase cells and later developmental stages (28). ForG encompasses 1,074 residues (European Nucleotide Archive data bank accession no. LN901451) and fully conforms to the canonical domain organization of DRFs (28). To assess a potential role of ForG in endocytosis, we expressed full-length (FL) and two truncated ForG constructs tagged with either green or yellow fluorescent protein (GFP/YFP) in the AX2 laboratory wild-type (WT) strain and monitored protein localization by confocal microscopy (Fig. 1*A* and Table S1). ForG-FL localized prominently to crowns and early endosomes, and also faintly to filopodia tips. In strong overexpressors (Fig. 1*A, Left)*, however, the localization was generally more diffuse, suggesting that endogenous GTPase levels became limiting to release ForG-FL from autoinhibition. Consistently, less diffuse distribution was observed with the constitutively active ForG variant (ForGΔDAD) lacking its C-terminal *Diaphanous*-autoregulatory domain (DAD). Because both constructs were formally able to catalyze excessive actin polymerization that might interfere with cell function, we additionally designed a truncated, N-terminal construct of ForG (ForG-N) encompassing the putative GBD at the very N terminus, followed by the FH3 domain (amino acids 1–423). Analogous constructs have previously been shown to be sufficient for intracellular targeting (25, 26, 29). As expected, ForG-N also faithfully localized to endocytotic structures but was no longer seen in filopodia tips. Moreover, when cup formation was physically inhibited by overlaying the cells with a thin sheet of agar, ForG-N accumulated at the leading edge of polarized cells (Fig. S1). Because we focused on endocytosis in the further course of this work, this construct was used for the localization studies.

Vegetative-phase cells, coexpressing LifeAct-mRPF as a marker for F-actin (30), revealed YFP–ForG-N to colocalize exclusively with F-actin–rich structures that formed macropinosomes (Fig. 1*B* and Movie S1). As opposed to the actin marker, which visualized actin-driven cell protrusions as well as the overall cortical F-actin, ForG was only enriched at the plasma membrane during the formation and maturation of macropinocytotic cups. Within a minute, these structures developed into endocytic vesicles filled with extracellular fluid that remained transiently decorated with ForG and F-actin before disassembly.

Next, we investigated whether phagocytosis of solid particles showed a similar spatiotemporal distribution of ForG. To assess this assumption, the uptake of TRITC-labeled yeast particles by *Dictyostelium* cells expressing YFP–ForG-N was monitored. Again, ForG-N localized to nascent phagocytic cups and remained associated with the membrane over the entire course of engulfment and internalization (Fig. 1*C* and Movie S2). In contrast to macropinosomes, however, the formation of phagosomes spanning several micrometers in diameter took considerably longer due to the large size of the yeast particles. Taken together, these localization experiments pointed toward a contribution of ForG in macropinocytosis and phagocytosis.

ForG Is Maximally Expressed in Vegetative Cells. Large-scale endocytosis occurs mainly in vegetative cells and during early development

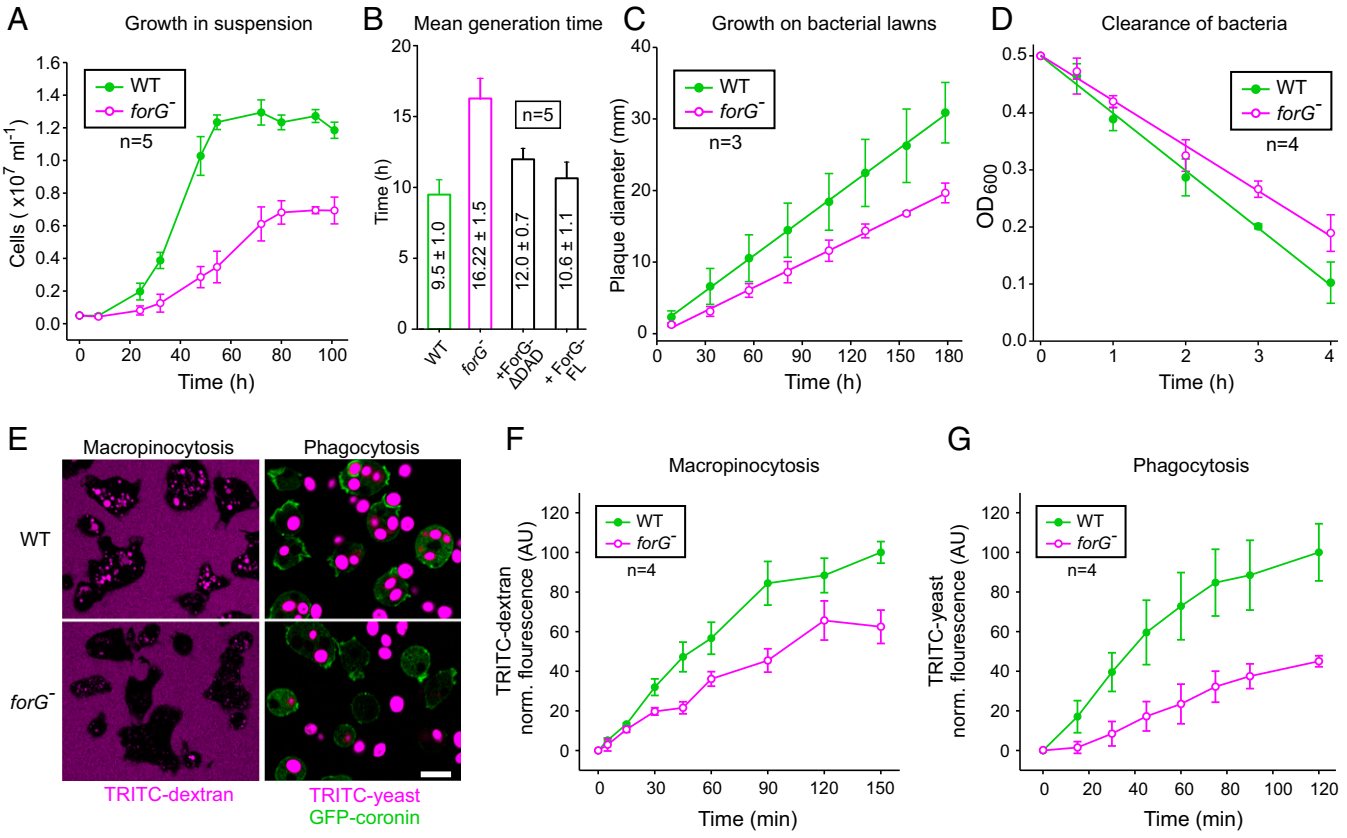

Fig. 3. Macropinocytosis and phagocytosis are impaired in *forG*$^-$ cells. (*A* and *B*) Growth of *forG*$^-$ cells in liquid medium was strongly reduced and resulted in an almost doubled mean generation time. Rescue with GFP–ForG-FL or GFP-ForGΔDAD almost restored WT rates (mean ± SD). (*C*) Plaque diameter on bacterial lawn was observed for several days and indicated a phagocytosis defect (mean ± SEM). (*D*) Clearance of bacteria from shaken suspension in the presence of WT or mutant cells revealed a 20% reduction of bacterial phagocytosis by *forG*$^-$ cells. (*E*) Accumulation of TRITC-dextran by macropinocytosis after 90 min of incubation and of TRITC-labeled yeast particles by phagocytosis after 30 min of incubation was visualized by confocal microscopy. (Scale bar: 10 μm.) (*F*) Quantification of macropinocytosis revealed decreased TRITC-dextran uptake in the *forG*$^-$ cells (mean ± SD). (*G*) Quantification of phagocytosis with TRITC-labeled yeast revealed markedly reduced uptake of large particles (mean ± SD). n, number of independent experiments.

(27). To validate our hypothesis, that ForG is involved in endocytosis, we set out to monitor its expression profile on the protein level and raised ForG-specific polyclonal antibodies directed against the C-terminal half of the protein (amino acids 562–1,074). Western blot analyses with total lysates from WT cells, collected at 3-h intervals from an entire developmental time course on filter pads, were probed for ForG and a battery of other marker proteins. ForG has a calculated molecular mass of 118.6 kDa but migrated at an apparent molecular mass of ∼130 kDa, most likely due to the presence of its proline-rich FH1 region as seen previously with other formins (31). Of note, ForG was maximally expressed in growth-phase cells and at the onset of starvation but then drastically dropped to low levels and remained more or less constant throughout the rest of the development (Fig. 2*A*, *Upper*). The drop occurred concomitantly with the appearance of the early developmental marker protein contact site A (csA) and clearly before the appearance of the prespore-specific antigen A (PsA) (32, 33). Taken together, these data therefore supported the notion that ForG is implicated in endocytosis.

Generation of ForG-Null Mutants. To study the physiological role of ForG in endocytosis, we next generated genetic KO mutants by homologous recombination. Successful gene disruption was initially assessed by diagnostic PCR using specific primer pairs and subsequently confirmed by Western blotting using the ForG antibodies (Fig. 2 *B* and *C*). This procedure allowed us to isolate multiple independent clones; however, because their phenotypes were indistinguishable, we used clone 10 in all later experiments, and henceforth refer to it as *forG*$^-$ cells. Based on this null mutant, we additionally generated reconstituted cell lines expressing ForG-FL and ForGΔDAD fused to GFP for further analyses (Fig. 2*D*).

ForG Is Required for Efficient Endocytosis. Next, we compared *forG*$^-$ and WT cells in a variety of nutrient uptake-dependent assays to evaluate the physiological role of ForG in endocytosis. Analysis of cell growth in shaken suspension with liquid medium revealed an almost doubled mean generation time for *forG*$^-$ cells of 16.2 ± 1.5 h (mean ± SD, n = 5) compared with WT cells, which required 9.5 ± 1.0 h (n = 5). Moreover, *forG*$^-$ cells only reached half-maximal cell density compared with control (Fig. 3 *A* and *B*). This effect was ForG-specific, because in *forG*$^-$ reconstituted cell lines expressing GFP-tagged ForG-FL or ForGΔDAD, the poor growth phenotype was largely reverted to WT values (Fig. 3*B*). We then assessed the growth of cells on bacterial lawns, which is mainly dependent on phagocytosis and subsequent digestion of nutrients. Notably, plaque growth as assessed by measuring its diameter over time was reduced by ∼33% to 0.111 ± 0.002 mm·h^{-1} in *forG*$^-$ cells as opposed to 0.166 ± 0.002 mm·h^{-1} for the WT (mean ± SEM, n = 3; Fig. 3*C*). Consistently, we observed diminished clearance of bacteria from shaken suspension culture by the mutant by about 20% (Fig. 3*D*). Impaired growth in shaken suspension or on bacterial lawns as seen with the *forG*$^-$ cells can occur due to poor uptake of nutrients as previously observed in PI3K multinull mutants and in KOs lacking their upstream activator Ras (15, 34), but it can also be caused by defects in cell division as shown for myosin II- or IBARa-null mutants (35, 36). However, due to the clear accumulation of ForG in macropinosomes and phagosomes, as well as the normal size of *forG*$^-$ cells in suspension, we reasoned that reduced nutrient uptake in the mutant cells was the most likely cause, and we therefore investigated fluid-phase and particle uptake in more detail. To this end, we first challenged *forG*$^-$ cells with the fluid-phase marker TRITC-dextran. Notably, after 90 min of incubation, a time point when equilibrium between TRITC-dextran accumulation via clathrin-independent endocytosis and exocytosis is normally reached (37), we observed substantially fewer and less brighter TRITC-dextran–containing vesicles in *forG*$^-$ cells as opposed to the WT (Fig. 3*E*, *Left*). Concurrently, we also examined phagocytosis of TRITC-labeled yeast particles by cells expressing GFP-coronin as a phagosome marker to visualize particle uptake in real time (18). Consistent with the reduced growth on bacteria, *forG*$^-$-derived cells accumulated only one to two yeast particles within a period of 30 min, whereas most WT cells were fully packed, containing multiple yeast particles (Fig. 3*E*, *Right*). Quantification of both macropinocytosis and phagocytosis over time corroborated these findings. The fluid-phase uptake rate in the *forG*$^-$ cells was reduced by 46% compared with controls (Fig. 3*F*). Moreover, the steady-state plateau was decreased by about one-third in the mutant. Quantification of phagocytosis in shaken suspension with TRITC-labeled yeast particles revealed similar results. The uptake rate of the *forG*$^-$ mutant cells was markedly reduced and reached only 55% of the WT value (Fig. 3*G*). Collectively, these data define ForG as a decisive factor of large-scale endocytosis.

ForG Does Not Substantially Affect Cell Migration. Previous work implied that endocytosis and cell migration are antagonistic processes because they require the same core machinery ultimately driving membrane protrusion (18, 38). To examine whether ForG is also implicated in migration, we compared the motility rates of WT and *forG*$^-$ cells in random motility assays. Surprisingly, the motile behavior of vegetative *forG*$^-$ cells was rather unaffected and did not noticeably deviate from WT motility regardless of the experimental conditions (Fig. 4*A*). In growth medium, the average speed of WT cells at 4.9 ± 1.9 μm·min^{-1} (mean ± SD, n = 546) was highly similar to *forG*$^-$ cells at 4.8 ± 2.5 μm·min^{-1} (n = 625). In low-osmolarity buffer, which is known to promote cell migration due to increased hydrostatic pressure (25), vegetative WT cells migrated only slightly faster (6.8 ± 2.6 μm·min^{-1}, n = 503) compared with *forG*$^-$ cells (6.0 ± 2.8 μm·min^{-1}, n = 536). These findings therefore argued against a general concept of inverse correlation between endocytosis and cell migration at that point. However, phalloidin labeling and phase-contrast time-lapse imaging of the cells revealed that *forG*$^-$ cells formed massively exaggerated actin-rich protrusions from large regions of their periphery as opposed to the WT, which formed mainly crowns and one or two pseudopods at a given time (Fig. 4*B* and Movie S3). Thus, although the loss of ForG strongly promotes the formation of actin-rich protrusions, this behavior does not seem to translate into increased cell motility, due to their excessive and uncoordinated nature.

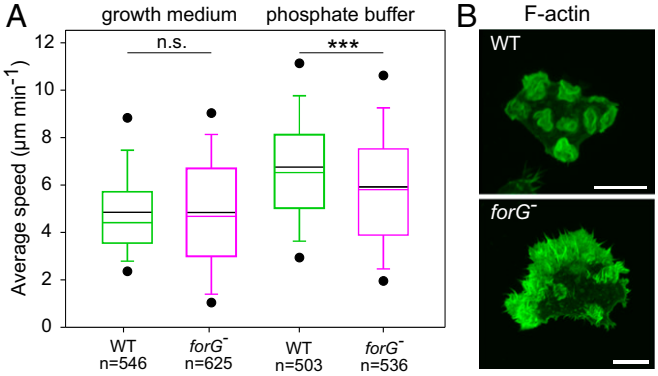

Fig. 4. Lack of ForG does not enhance motility but drives excessive formation of actin-rich cell protrusions. (*A*) Box plot summarizing quantitative analysis of random cell migration of WT and *forG*$^-$ cells in growth medium and low-osmolarity Sorensen's buffer. Note similar random motility rates for both strains in both conditions. Boxes indicate the 25th through 75th percentiles, the whiskers mark the 10th and 90th percentiles, and the outliers mark the fifth and 95th percentiles. Black solid lines indicate mean values. n, number of tracked cells. ***P < 0.001 (Mann–Whitney U test). n.s., nonsignificant. (*B*) Loss of ForG results in strikingly exaggerated actin-rich protrusion (Movie S3). The cells indicated were cultivated in growth medium, fixed, and stained for F-actin with ATTO488-conjugated phalloidin. (Scale bar: 10 μm.)

ForG Promotes F-Actin Assembly. The core FH1-FH2 domains of canonical formins catalyze the nucleation and processive elongation of linear F-actin filaments, but their specific activities can be highly diverse (39). Thus, to assess the potential function of ForG in endocytosis, we expressed and purified two recombinant C-terminal ForG fragments for biochemical analysis. The larger construct comprises all three polyproline stretches of the FH1 domain (ForG-3P), and the shorter ForG-1P construct contains just the last stretch adjacent to the FH2 domain (Fig. 5*A*). Bulk polymerization assays with pyrene-actin and increasing amounts of ForG-3P in the nanomolar range revealed that ForG stimulated spontaneous actin assembly in a concentration-dependent manner (Fig. 5*B*), albeit less strongly compared with a C-terminal ForE fragment (ForE-4P), which was used as a reference (31). Next, both ForG fragments and ForE-4P were analyzed with regard to their nucleation activity by total internal reflection fluorescence microscopy (TIRFM) on the single-filament level (Fig. 5*C*). As opposed to other formins, such as *Dictyostelium* ForE or mDia2 (26), at 10 nM concentrations, both ForG fragments only moderately enhanced the birth of new actin filaments, indicative of a rather weak nucleation activity (Fig. 5*D*). Then, we analyzed the filament elongation in the TIRFM assay. In the presence of *Dictyostelium* PFN I, both ForG-1P and ForG-3P promoted barbed-end elongation by about threefold to 33.4

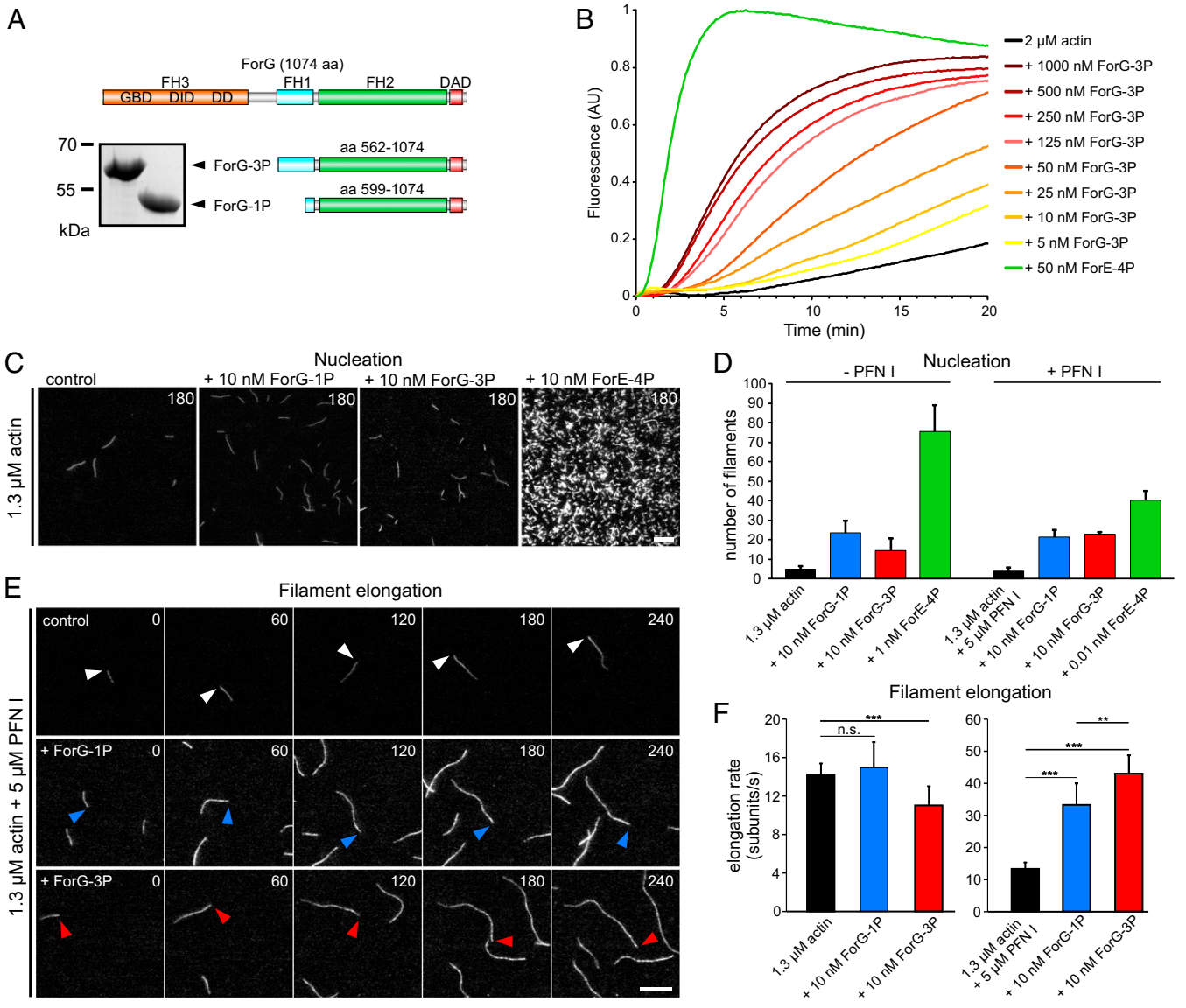

Fig. 5. ForG promotes F-actin assembly. (*A*) Domain organization of ForG and derived C-terminal constructs used for biochemical analyses. (*Inset*) Purified ForG-1P and ForG-3P fragments. (*B*) ForG-3P promoted polymerization of pyrene-labeled G-actin (2 µM, 5% labeled) in a concentration-dependent manner. Note markedly higher assembly rates by 50 nM ForE-4P. AU, arbitrary units. (*C*) ForG exhibits rather weak actin filament nucleation compared with ForE-4P. Representative frames from TIRFM time-lapse recordings of actin filament assembly are shown. (*D*) Nucleation efficacies of ForG and ForE constructs in the absence or presence of PFN I (mean ± SD, $n = 3$). Note that due to the strong nucleation efficacy, and for technical reasons, 10- or 1,000-fold less of ForE-4P had to be used for the quantifications. (*E*) Filament elongation visualized by TIRFM in the presence of 5 µM PFN I alone or in combination with either 10 nM ForG-1P or 10 nM ForG-3P. Barbed ends are marked by arrowheads. Time is given in seconds. (*F*) Elongation rates of growing filaments were calculated from time-lapse movies as shown in *E*. (*Left*) In the absence of PFN I, addition of 10 nM ForG-3P led only to slightly reduced elongation compared with rates of control and ForG-1P. (*Right*) In the presence of PFN I, ForG-1P– and ForG-3P–associated filaments were elongated about threefold faster than control filaments (mean ± SD). At least 20 individual filaments were tracked. ***$P \leq 0.001$, **$P \leq 0.01$ (Mann-Whitney *U* test). Note that the scale differs between the left and right graphs. (Scale bars: *C*, 5 µm; *E*, 10 µm.)

and 43.1 subunits per second, respectively, compared with the actin control with 13.4 subunits per second (Fig. 4 *E* and *F* and Movie S4). The higher activity of ForG-3P emphasized more efficient PFN-actin recruitment by its two additional polyproline stretches and is consistent with previous work (31, 40). In the absence of PFN, formins can reside as leaky cappers on the growing filament barbed ends and may suppress their growth significantly (41). Interestingly, impaired growth was not seen with ForG-1P, and ForG-3P showed just slightly reduced filament elongation at a concentration of 10 nM from 14.2 to 11 subunits per second (Fig. 5*F*). Extended biochemical analyses by additional pyrene, as well as low-speed and high-speed sedimentation assays, further revealed that ForG efficiently competes with *Dictyostelium* capping protein Cap32/34 (CP) for filament barbed ends. By determining the dissociation constant of CP for filament ends (0.53 ± 0.07 nM; Fig. S2), we were able to calculate the affinity of ForG for filament barbed ends from competition experiments in presence of CP to 4.4 ± 1.1 nM (Fig. S2). Thus, ForG is a leaky capper that allows incorporation, as well as the release, of monomers even when tightly bound to

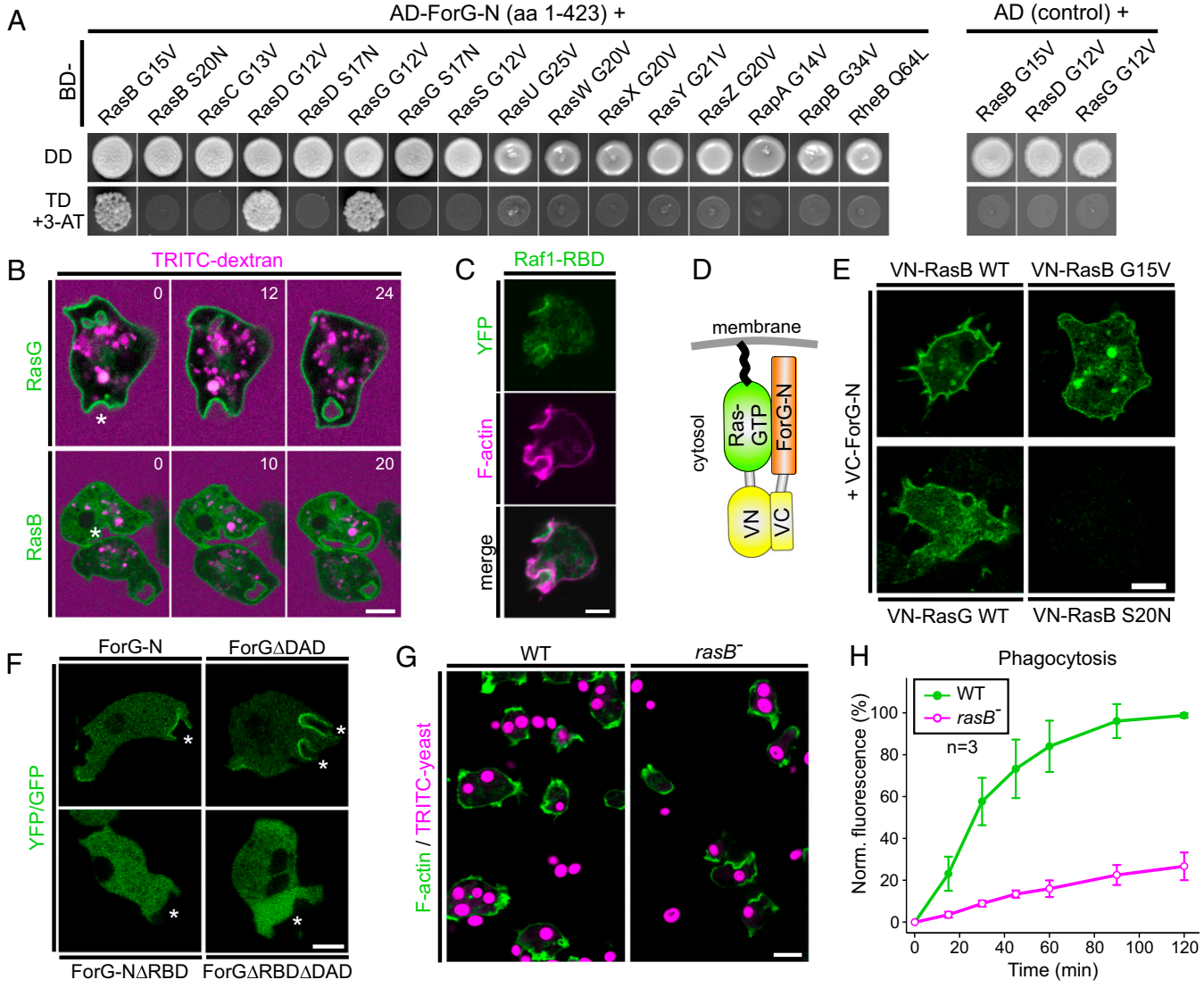

Fig. 6. ForG interacts with active Ras. (*A*, *Left*) ForG-N interacts specifically with the active forms of RasB, RasG, and RasD in the Y2H assay. Yeast was transformed with the indicated constructs and selected for the presence of prey and bait plasmids by growth on double-dropout (DD) media lacking leucine and tryptophan. Interactions were assayed by growth on stringent triple-dropout (TD) media additionally lacking histidine in the presence of 3 mM 3-AT. (*A*, *Right*) Three identified Ras proteins showed no genetic interaction in experiments using the dominant-negative Ras variants or empty AD plasmids as negative controls. AD, Gal4-activation domain; 3-AT, 3-amino-1,2,4-triazole; BD, Gal4-binding domain. (*B*) YFP-tagged RasG and RasB also localize to macropinosomes during the uptake of TRITC-dextran–labeled medium. Confocal sections are shown and correspond to Movies S5 and S6. Time is given in seconds. Macropinosomes are indicated by stars. (*C*) Macropinosomes contain active Ras proteins as evidenced by accumulation of the pan-Ras probe Raf1-RBD. A confocal section of a live-cell coexpressing YFP-tagged Raf1-RBD and the F-actin probe LifeAct-mRFP is shown. (*D*) Scheme of the BiFC strategy. VC, Venus C-terminal fragment; VN, Venus N-terminal fragment. (*E*) ForG-N interacted with active or WT forms of RasB and RasG, but not with the dominant-negative control of RasB in the BiFC assay. Representative confocal sections are shown. (*F*) Removal of the putative RBD in ForG-N and the constitutively active ForGΔDAD variant abolished localization of the fusion proteins at endocytic cups (white stars). (*G*) Strongly impaired yeast phagocytosis of *rasB*$^{-}$ cells. Accumulation of TRITC-labeled yeast particles by phagocytosis after 45 min of incubation on glass coverslips. Confocal sections are shown. (*H*) Quantification of phagocytosis with TRITC-labeled yeast revealed strikingly reduced uptake of large particles (mean ± SD, $n = 3$ for each cell line). Norm., normalized. (Scale bars: *B*–*F*, 5 μm; *G*, 10 μm.)

barbed ends. Because ForG also neither bundles filaments nor binds to their sides (Fig. S2), these data therefore pointed toward a central role of ForG in filament elongation during large-scale endocytosis.

ForG Interacts with Active Ras Proteins. To date, DRFs have been shown to act exclusively as effectors of the Rho-family GTPases, such as Cdc42, Rho, and Rac (24). We therefore explored which GTPase could be responsible for activation of ForG by a yeast two-hybrid (Y2H) screen, using the N-terminal ForG fragment ForG-N encompassing the GBD and the FH3 region (amino acids 1–423) as bait. Although *Dictyostelium* cells lack genuine Rho and Cdc42 homologs, they express 20 Rac-subfamily GTPases (42). Thus, we systematically screened ForG-N with all these Rac GTPases in their constitutively activated forms obtained by amino acid substitutions corresponding either to position 12 within the P-loop or to position 61 within switch II of human Rac1, respectively (43, 44) (Table S2). However, despite false-positive hits with RacM and RacH, we failed to find any interaction with a Rac GTPase in this Y2H screen (Fig. S3). Of note, ForG contains a putative ubiquitin-like fold that, despite lack of sequence homology, represents structurally conserved topology of many Ras-binding domains (RBDs) in Ras-effectors, such as proteins from the MAP kinase pathway (45) or PI3Ks (46). Because Ras proteins are also intimately linked to endocytosis (3, 15), in a second Y2H screen, we used all members of the annotated Ras GTPase subfamily as prey except for RasV, which bears an N-terminal poly-N stretch, and RapC, which lacks the conserved nucleotide-binding sites (47). Strikingly, we found ForG-N to interact specifically with the activated forms of RasB, RasG, and RasD, but not with their dominant-negative variants (Fig. 6*A*). All these Ras proteins show high sequence homologies to the human KRas and HRas proto-oncogenes, but because RasD is exclusively expressed at later developmental stages (48) during which endocytosis has been largely shut down, these data imply that ForG is only regulated by RasG and RasB in vivo. Taken together, these unexpected results pointed toward a direct activation of a DRF by Ras proteins, which have long been considered important orchestrators of endocytosis and cell migration (15).

Although the role of RasG in endocytosis is well established (15), much less is known about RasB. We therefore compared the in vivo localization and dynamics of fluorescently tagged RasB and compared it with an analogous RasG fusion construct. Both GTPases localized prominently to the plasma membrane and also to invaginations that eventually developed into macropinosomes as assessed by the capture of the fluid-phase marker TRITC-dextran (Fig. 6*B*). To visualize active Ras in cells, we then used the RBD of Raf1 fused to YFP and found it to colocalize with F-actin in endocytic cups (Fig. 6*C*). The RBDs of mammalian Raf1 or of yeast Byr2 kinases are commonly used pan-Ras probes (49), and they consistently also interact with numerous active *Dictyostelium* GTPases, including RasB and RasG as evidenced by Y2H assays (Fig. S4). These findings therefore supported the notion that active RasG and RasB accumulate in the cups and act as regulators of ForG in endocytosis.

Unfortunately and despite numerous attempts, we were not able to purify a soluble N-terminal ForG fragment for in vitro interaction studies with recombinant RasB and RasG. Nevertheless, to corroborate the interaction of RasG and RasB with ForG in an independent assay, we first adapted in vivo bimolecular fluorescence complementation (BiFC) of the YFP variant Venus for use in *Dictyostelium* (Fig. 6 *D* and *E*). To this end, an extrachromosomal vector for the simultaneous expression of two proteins was constructed with split Venus fragments that eliminate self-complementation, and therefore provide high specificity as reported by Ohashi et al. (50), who conducted systematic fragment pair optimization and demonstrated active H-Ras and Raf1 interaction. When the BiFC construct was expressed in *forG*$^-$ mutants to circumvent unconstructive interaction of ectopic RasB with endogenous ForG, most cells showed rather weak but distinct fluorescence enrichment at the plasma membrane. We assumed this weak fluorescence enrichment was due to the maturation of split Venus, which takes minutes to hours (51) and evidently exceeds the rather short time frame of Ras activation during macropinocytosis, which is completed within 1 min (15) (Fig. 1*B*). Because Venus is quite stable once assembled, some cells accumulated a stronger fluorescence at the plasma membrane several days after transfection, as shown in Fig. 6*E*. Notably, fluorescence complementation was seen with WT as well as constitutively active RasB, but never with dominant-negative RasB (Fig. 6*E*). Because similar results were also obtained with RasG-WT, these data demonstrated that active RasB and RasG specifically interact with ForG in vivo. Finally, we asked whether Ras binding is required for ForG localization to endocytic cups. To this end, we expressed truncated variants of ForG-N and ForGΔDAD additionally lacking the putative RBD (amino acids 1–119). Notably, as shown in Fig. 6*F*, cup localization was abolished with both of these constructs, demonstrating that the RDB is essential for subcellular targeting.

RasB-Null Cells Exhibit Severe Defects in Phagocytosis. As opposed to RasG, the function of RasB in endocytosis has not yet been examined. Thus, we generated a cell line devoid of RasB by homologous recombination (Fig. S5) and assayed a number of growth parameters depending on large-scale endocytosis. In comparison to WT cells, *rasB*$^-$ cells grew slightly slower in shaken suspension containing growth medium, but exhibited only weakly diminished pinocytosis rates (Fig. S6). However, the uptake of large particles was substantially impaired (Fig. 6 *G* and *H*), although the phagocytosis of bacteria was only moderately reduced (Fig. S6). Therefore, *rasB*$^-$ cells especially appear to exhibit major defects in phagocytosis of large objects.

Impaired F-Actin Accumulation in Phagosomes of *forG*$^-$ Mutants. To assess potential defects in actin assembly during large-scale endocytosis, we then visualized the F-actin distribution in semi-closed phagosomes of *forG*$^-$ and *rasB*$^-$ mutants engulfing yeast and compared them with control cells as well as the phagocytosis-impaired mutant lacking the Arp2/3 complex activator SCAR (52, 53). Whereas F-actin was more or less evenly distributed in WT cells around the entire phagocytic cup engulfing the yeast particles, we observed striking abnormalities in the F-actin distribution in *forG*$^-$ cells (Fig. 7*A*). The latter characteristically contained a markedly weaker F-actin signal at the base of forming phagosomes and occasionally also displayed asymmetries in the distribution of F-actin in the tip region. Because all images were obtained with identical microscope settings, we plotted the phalloidin fluorescence intensities along the contour of the nascent phagosomes to quantify the F-actin content in these structures. This analysis revealed a 47% reduction of F-actin in the base of the phagosomes of *forG*$^-$ cells (Fig. 7*B*, *Left*), which is consistent with ForG-mediated actin assembly in vitro. The analysis of the *rasB*$^-$ mutant revealed an intermediate actin reduction in the cup base by 26% (Fig. 7*B*, *Middle*) compared with the WT and *forG*$^-$ cells. Thus, it appears that ForG is only partly activated in this cell line, which is consistent with the notion that ForG is most likely also activated by RasG. Analysis of *scrA*$^-$ cells interestingly revealed only a minor reduction by 13% in the base, but the strongest F-actin reduction of all analyzed cell lines by about 24% at the rim of the cups (Fig. 7*B*, *Right*). Moreover, *scrA*$^-$ cells displayed aberrant cup morphology, as if these mutants were not able to grasp the yeast particles tightly. Consistently, and as opposed to all other cell lines, we frequently found many empty cups in fixed cells (Fig. 7*A*, *Lower Right*). Finally, we performed confocal time-lapse imaging with the GFP-tagged F-actin probe LimEΔcoil to monitor F-actin

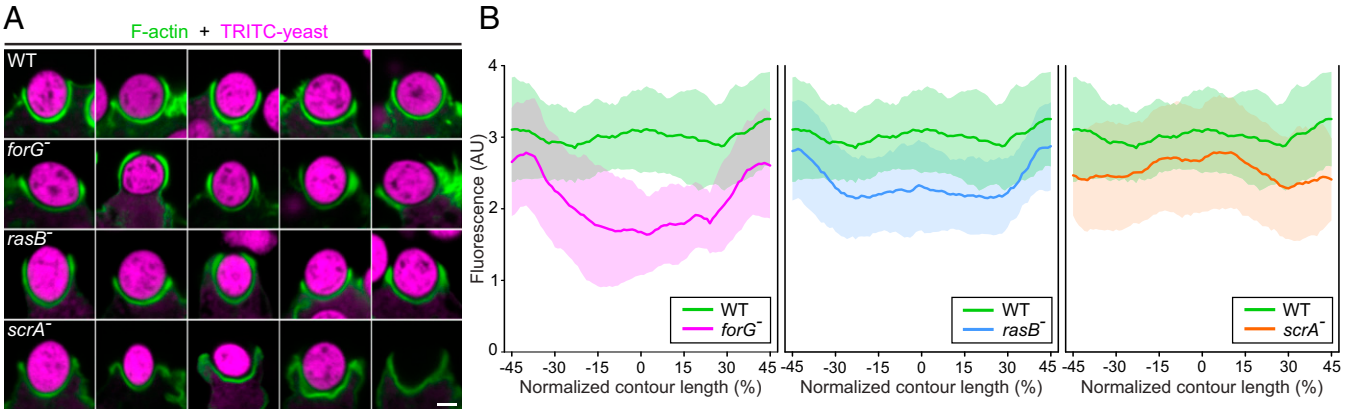

Fig. 7. Aberrant F-actin distribution in phagosomes of cells impaired in phagocytosis. (*A*) Representative phagosomes from WT cells (first row) and the *forG*$^{-}$ mutant cells (second row), *rasB*$^{-}$ cells (third row), and *scrA*$^{-}$ cells (fourth row). Growth-phase cells phagocytosing TRITC-labeled yeast particles were fixed and stained for F-actin with ATTO488-conjugated phalloidin. Note impaired F-actin distribution in the mutant cells and empty cups in *scrA*$^{-}$ cells (fourth row) suggesting loose association with the yeast particles. (Scale bar: 2 μm.) (*B*) Quantification of the relative F-actin contents in the phagosomes of WT and mutant cells. Fluorescence intensities of the ATTO488 phalloidin-labeled F-actin structure along the contour lengths of phagosomes are shown (mean ± SD). The base of the phagosomes was set to 0% (n = 25 for each cell line). AU, arbitrary units.

dynamics throughout the phagocytosis cycle in live cells. These recordings are consistent with the still images of Fig. 7*A* and corroborated, in particular, the problem of *scrA*$^{-}$ cells initiating cup formation and constricting the rim during phagosome maturation (Movies S7–S10). Together, these findings suggest a synergy between the Arp2/3 complex and ForG-generated actin networks to drive efficient engulfment of large particles.

Discussion

D. discoideum is a professional phagocyte that feeds on bacteria or yeast in the soil. For the ease of cultivation, axenic laboratory strains have been engineered that are also able to internalize large quantities of bulk fluid due to greatly enhanced macropinocytosis (10). Nevertheless, both processes share many similarities and components because, in both cases, the dynamic assembly of actin filaments together with myosins generates forces that drive internalization of fluid or large particles. Moreover, they are of high medical relevance because, in the immune defense, phagocytosis is a major mechanism to remove pathogens (7), whereas many cancer cells thrive by excessive macropinocytosis (3, 5). Recent work with *Dictyostelium* showed that the nucleation-promoting factor SCAR/WAVE localizes at the very rim of macropinosomes, suggesting that the Arp2/3 complex acts as a potent nucleator of the underlying actin filament network (38). Consistently, the Arp2/3 complex was also shown to be required for large-scale endocytosis in higher eukaryotes (54). Formins, such as the DRFs mDia1, FMNL1/FRL1, and Daam1 (29, 55–57), have also been implicated in phagocytosis in immune cells, albeit the molecular function of these actin assembly factors is less clear.

In this study, we aimed to characterize the function of the *Dictyostelium* DRF ForG that regulates specifically the dynamic reorganization of the actin cytoskeleton in large-scale endocytosis. Interestingly, we found ForG to decorate the entire actin-rich base of nascent phagosomes and macropinosomes throughout their entire lifetime. This observation is reminiscent of the localization of coronin, which is an indicative marker of highly dynamic actin filament networks, such as phagosomes or lamellipodia (18, 58), in which it acts as a potent enhancer of cofilin-mediated filament disassembly (20). More importantly, our in vitro experiments revealed a rather weak nucleation activity by ForG, whereas filament elongation in the presence of PFN was increased about threefold at 1.3 μM actin in the TIRFM assay. Given the much higher actin concentration in cells, these data imply that ForG acts as an effective actin filament elongator that contributes to the generation of a functional F-actin network in endocytosis. Consistently, we observed substantially reduced amounts of F-actin, particularly at the base of phagocytic cups in *forG*$^{-}$ cells, which correlated with severe defects in large-scale endocytosis. Similarly, *scrA*$^{-}$ cells also have reduced F-actin levels in the cups and were previously shown to have significantly reduced rates of macropinocytosis (52). Most notably, deletion of SCAR in the PFN-null background resulted in a further substantial decrease in endocytosis compared with either mutant alone, suggesting that PFN and SCAR both functionally contribute to regulate endocytosis (52). However, at that time, the molecular mechanism of formins was not well enough understood to interpret these findings. However, in light of this study and our current knowledge about formin function, these data can now be easily explained by the synergistic action of the nucleating Arp2/3 complex and the filament-elongating activity of a formin, because the latter requires PFN to achieve fast filament elongation (39, 40, 59). Thus, ForG may operate in elongation of Arp2/3 complex-nucleated filaments to establish a robust actin meshwork allowing efficient membrane protrusion and internalization of extracellular material. This synergistic mode of action between different actin assembly factors has been proposed for actin polymerization in lamellipodia, in which Arp2/3 complex-generated filaments are captured by the DRF FMNL2 to promote their elongation in a PFN/actin-dependent manner to drive efficient cell migration (60). Of note, the Arp2/3 complex and the DRFs mDia1 and FMNL1 also seem to synergize during a specialized form of internalization of *Borrelia burgdorferi* by macrophages, termed coiling phagocytosis (56), meaning that this type of cooperation between different actin assembly factors may be a general concept in various actin-based processes.

However, if filament elongation is equally critical for macropinocytosis and phagocytosis, and provided that ForG is the only formin involved, why then is large-scale endocytosis in *forG*$^{-}$ cells not entirely blocked? Pioneering work on the requirement of the minimal set of proteins in actin-based cell motility in reconstituted systems led to the identification of actin, capping protein, ADF/cofilin, and the Arp2/3 complex as the only essential actin assembly factors (61). However, when the filament elongator VASP was added to these critical components, the speed of *Listeria* was accelerated 2.5-fold in vitro. These findings are therefore consistent with the ∼50% reduction of large-scale endocytosis in *forG*$^{-}$ cells and illustrate that coupling of an actin filament nucleator with an actin polymerase optimizes efficiency.

The initial steps of phagocytosis have been extensively studied and seem to be triggered by the recently identified folate receptor

fAR1 (12) and its associated heterotrimeric G protein (13) to activate a subset of Ras proteins, which, in turn, leads to activation of their class-1 PI3K downstream effectors and production of PIP_3 (34, 62). Due to a mutation of the RasGAP neurofibromin NF1, in axenic *Dictyostelium* strains, excessive Ras signaling appears to bypass the requirement for fAR1-receptor activation and makes macropinocytosis constitutive, allowing the cells to grow efficiently in liquid medium (10). The links between PIP_3 and the cytoskeleton are not yet fully resolved, but several downstream effectors of this phosphoinositide, including RacGEFs and Akt, have been proposed to lead to activation of Arp2/3 complex-mediated actin assembly (63, 64).

Previous work demonstrated that mutants lacking PI3Ks and the small GTPases RasG and RasS display a significantly decreased large-scale endocytosis, thus supporting the view that these proteins operate in a common signaling pathway (15, 34). However, the specific impact of these proteins on the two types of large-scale endocytosis is not always identical (15). In addition, seemingly unrelated phenotypes, such as the cytokinesis defect of *rasG*$^-$ cells (65), make the dissection of the underlying pathways a challenging task. Notwithstanding these findings, a shared inventory of core components must be at play, which can be complemented by additional factors that preferentially engage in either macropinocytosis or phagocytosis. In this work, we identify a formin that interacts with RasG and RasB, thus directly linking Ras GTPase signaling with actin polymerization in large-scale endocytosis. Because *forG*$^-$ cells displayed severe defects in both fluid-phase and solid particle uptake, we propose ForG to be part of the core machinery. Based on a rather weak impairment of macropinocytosis in *rasB*$^-$ cells but a strong impact on phagocytosis, this study further suggests that RasB is mainly responsible for activation and recruitment of ForG during phagocytosis of large particles, whereas RasG is the main regulator in macropinocytosis.

The interaction of active Ras with the N-terminal GBD of ForG is expected to recruit ForG to crown-shaped protrusions and release the intrinsic autoinhibition to drive elongation of actin filaments after their nucleation by the Arp2/3 complex. Consistent with previous localization studies with mDia1 (29), the GBD of ForG was found to be critical for subcellular targeting. Moreover, based on the close sequence relationship of the ForG-GBD with the N terminus of the developmentally regulated DRF ForC (26), which, in turn, was shown to interact with PIP_3 (66), we hypothesized that PIP_3 may additionally support targeting of ForG to endocytic cups. Unfortunately, we were not able to purify a soluble ForG fragment from *E. coli* to test Ras and lipid interactions in vitro. Nevertheless, treatment of cells with the PI3K inhibitor LY2904002 at 25 μM or 50 μM was sufficient to delocalize ForG-N completely from the membrane and render it entirely cytosolic, whereas the Arp2/3 inhibitor CK666 had no effect (Fig. S7). Together, these findings support the view that PIP_3, together with active Ras but not the Arp2/3 complex or interaction with F-actin (Fig. 1*A*), is required for ForG targeting.

Of note, the tertiary structure of the ForC-GBD was shown to adapt an ubiquitin-like fold (66), which is, when combined with positively charged patches at the interaction surface, a hallmark of RBDs (45). In higher eukaryotes, the closest homologs of ForG are members of the FHOD family (28), which are actin-bundling proteins mainly found in stress fibers (67). Intriguingly, the crystal structure of the FHOD1-GBD also adapts an ubiquitin-like superfold (68). However, because FHOD1 lacks the positively charged residues, it fails to interact with active Ras, so that insertion of one lysine residue (P41K) is required to allow for moderate interaction with Ras (68). Moreover, FHOD1 was previously shown to be regulated by the Rho-dependent protein kinase ROCK, which releases the autoinhibition by phosphorylation of the DAD (67). Except for the dedicated phagocytes of the innate immune system, which clear pathogens, most vertebrate cells do not perform large-scale endocytosis. These findings therefore suggest that the ancestral FHOD-like formin in vertebrates might have evolved from a Ras-regulated formin to a Rho-regulated factor implicated in novel activities, such as stress fiber formation (67), whereas in *Dictyostelium* cells, the Ras regulation of this formin remained evolutionary conserved to preserve a direct link to actin assembly in large-scale endocytosis. Interestingly however, hyperactive Ras signaling in cancer from various origins might awaken the ancestral feeding mechanisms of large-scale endocytosis from dormancy in the form of excessive macropinocytosis. Thus, although the core machineries appear conserved, the unraveling of similarities and differences between amoeba and mammalian cells poses a challenging but fascinating task for the future.

Materials and Methods

A complete description of the methods is provided in *SI Materials and Methods*. This description includes construction of plasmids and *Dictyostelium* mutants, protein purification and labeling, actin assembly assays, antibodies and immunoblots, fluorescence microscopy and imaging, analyses of the F-actin distribution in phagocytic cups, endocytosis assays, analyses of cell migration, Y2H assays, and statistical analysis.

ACKNOWLEDGMENTS. We thank Annette Breskott for technical assistance and all members of the group for stimulating discussions. Furthermore, we are grateful to Matthias Preller for suggestions in BiFC linker design, Sarah Körber for assistance in Y2H screens, Ludwig Eichinger for providing prespore antigen A antibody, the Dicty Stock Center, and depositor Douwe Veltman for supplying us with pDM plasmids. This work was supported by Deutsche Forschungsgemeinschaft Grants FA 330/6-2 and FA 330/10-1 (to J.F.). V.F. was supported by the FP7-REGPOT-2012-2013-1 Grant Agreement 316289–InnoMol.

1. Mayor S, Pagano RE (2007) Pathways of clathrin-independent endocytosis. *Nat Rev Mol Cell Biol* 8(8):603–612.
2. Rougerie P, Miskolci V, Cox D (2013) Generation of membrane structures during phagocytosis and chemotaxis of macrophages: Role and regulation of the actin cytoskeleton. *Immunol Rev* 256(1):222–239.
3. Commisso C, et al. (2013) Macropinocytosis of protein is an amino acid supply route in Ras-transformed cells. *Nature* 497(7451):633–637.
4. Kamphorst JJ, et al. (2013) Hypoxic and Ras-transformed cells support growth by scavenging unsaturated fatty acids from lysophospholipids. *Proc Natl Acad Sci USA* 110(22):8882–8887.
5. Bloomfield G, Kay RR (2016) Uses and abuses of macropinocytosis. *J Cell Sci* 129(14):2697–2705.
6. Swanson JA (2008) Shaping cups into phagosomes and macropinosomes. *Nat Rev Mol Cell Biol* 9(8):639–649.
7. Levin R, Grinstein S, Canton J (2016) The life cycle of phagosomes: Formation, maturation, and resolution. *Immunol Rev* 273(1):156–179.
8. Veltman DM, Lemieux MG, Knecht DA, Insall RH (2014) PIP_3-dependent macropinocytosis is incompatible with chemotaxis. *J Cell Biol* 204(4):497–505.
9. Sussman R, Sussman M (1967) Cultivation of Dictyostelium discoideum in axenic medium. *Biochem Biophys Res Commun* 29(1):53–55.
10. Bloomfield G, et al. (2015) Neurofibromin controls macropinocytosis and phagocytosis in Dictyostelium. *eLife* 4:1–25.
11. Maniak M (2002) Conserved features of endocytosis in Dictyostelium. *Int Rev Cytol* 221:257–287.
12. Pan M, Xu X, Chen Y, Jin T (2016) Identification of a chemoattractant G-protein-coupled receptor for folic acid that controls both chemotaxis and phagocytosis. *Dev Cell* 36(4):428–439.
13. Hoeller O, et al. (2016) Gβ regulates coupling between actin oscillators for cell polarity and directional migration. *PLoS Biol* 14(2):e1002381.
14. Cai H, et al. (2010) Ras-mediated activation of the TORC2-PKB pathway is critical for chemotaxis. *J Cell Biol* 190(2):233–245.
15. Hoeller O, et al. (2013) Two distinct functions for PI3-kinases in macropinocytosis. *J Cell Sci* 126(Pt 18):4296–4307.
16. Clark J, et al. (2014) Dictyostelium uses ether-linked inositol phospholipids for intracellular signalling. *EMBO J* 33(19):2188–2200.
17. Clarke M, et al. (2010) Curvature recognition and force generation in phagocytosis. *BMC Biol* 8(1):154.
18. Maniak M, Rauchenberger R, Albrecht R, Murphy J, Gerisch G (1995) Coronin involved in phagocytosis: Dynamics of particle-induced relocalization visualized by a green fluorescent protein Tag. *Cell* 83(6):915–924.
19. Konzok A, et al. (1999) DAip1, a Dictyostelium homologue of the yeast actin-interacting protein 1, is involved in endocytosis, cytokinesis, and motility. *J Cell Biol* 146(2):453–464.
20. Mikati MA, Breitsprecher D, Jansen S, Reisler E, Goode BL (2015) Coronin enhances actin filament severing by recruiting cofilin to filament sides and altering F-actin conformation. *J Mol Biol* 427(19):3137–3147.
21. Swanson JA, et al. (1999) A contractile activity that closes phagosomes in macrophages. *J Cell Sci* 112(Pt 3):307–16.

22. Brzeska H, Koech H, Pridham KJ, Korn ED, Titus MA (2016) Selective localization of myosin-I proteins in macropinosomes and actin waves. *Cytoskeleton (Hoboken)* 73(2):68–82.
23. Vinzenz M, et al. (2012) Actin branching in the initiation and maintenance of lamellipodia. *J Cell Sci* 125(Pt 11):2775–2785.
24. Pollard TD (2007) Regulation of actin filament assembly by Arp2/3 complex and formins. *Annu Rev Biophys Biomol Struct* 36:451–477.
25. Ramalingam N, et al. (2015) A resilient formin-derived cortical actin meshwork in the rear drives actomyosin-based motility in 2D confinement. *Nat Commun* 6:8496.
26. Junemann A, et al. (2013) ForC lacks canonical formin activity but bundles actin filaments and is required for multicellular development of Dictyostelium cells. *Eur J Cell Biol* 92(6-7):201–212.
27. Katoh M, Chen G, Roberge E, Shaulsky G, Kuspa A (2007) Developmental commitment in Dictyostelium discoideum. *Eukaryot Cell* 6(11):2038–2045.
28. Rivero F, et al. (2005) A comparative sequence analysis reveals a common GBD/FH3-FH1-FH2-DAD architecture in formins from Dictyostelium, fungi and metazoa. *BMC Genomics* 6:28.
29. Seth A, Otomo C, Rosen MK (2006) Autoinhibition regulates cellular localization and actin assembly activity of the *Diaphanous*-related formins FRLalpha and mDia1. *J Cell Biol* 174(5):701–713.
30. Riedl J, et al. (2008) Lifeact: A versatile marker to visualize F-actin. *Nat Methods* 5(7): 605–607.
31. Winterhoff M, et al. (2014) The Diaphanous-related formin dDia1 is required for highly directional phototaxis and formation of properly sized fruiting bodies in Dictyostelium. *Eur J Cell Biol* 93(5-6):212–224.
32. Noegel A, Gerisch G, Stadler J, Westphal M (1986) Complete sequence and transcript regulation of a cell adhesion protein from aggregating Dictyostelium cells. *EMBO J* 5(7):1473–1476.
33. Krefft M, Voet L, Gregg JH, Mairhofer H, Williams KL (1984) Evidence that positional information is used to establish the prestalk-prespore pattern in Dictyostelium discoideum aggregates. *EMBO J* 3(1):201–206.
34. Chubb JR, Wilkins A, Thomas GM, Insall RH (2000) The Dictyostelium RasS protein is required for macropinocytosis, phagocytosis and the control of cell movement. *J Cell Sci* 113(Pt 4):709–719.
35. De Lozanne A, Spudich JA (1987) Disruption of the Dictyostelium myosin heavy chain gene by homologous recombination. *Science* 236(4805):1086–1091.
36. Linkner J, et al. (2014) The inverse BAR domain protein IBARa drives membrane remodeling to control osmoregulation, phagocytosis and cytokinesis. *J Cell Sci* 127(Pt 6): 1279–1292.
37. Klein G, Satre M (1986) Kinetics of fluid-phase pinocytosis in Dictyostelium discoideum amoebae. *Biochem Biophys Res Commun* 138(3):1146–1152.
38. Veltman DM (2015) Drink or drive: Competition between macropinocytosis and cell migration. *Biochem Soc Trans* 43(1):129–132.
39. Kovar DR, Harris ES, Mahaffy R, Higgs HN, Pollard TD (2006) Control of the assembly of ATP- and ADP-actin by formins and profilin. *Cell* 124(2):423–435.
40. Paul AS, Pollard TD (2008) The role of the FH1 domain and profilin in formin-mediated actin-filament elongation and nucleation. *Curr Biol* 18(1):9–19.
41. Kovar DR, Kuhn JR, Tichy AL, Pollard TD (2003) The fission yeast cytokinesis formin Cdc12p is a barbed end actin filament capping protein gated by profilin. *J Cell Biol* 161(5):875–887.
42. Vlahou G, Rivero F (2006) Rho GTPase signaling in Dictyostelium discoideum: Insights from the genome. *Eur J Cell Biol* 85(9-10):947–959.
43. Bishop AL, Hall A (2000) Rho GTPases and their effector proteins. *Biochem J* 348(Pt 2):241–255.
44. Steffen A, Koestler SA, Rottner K (2014) Requirements for and consequences of Rac-dependent protrusion. *Eur J Cell Biol* 93(5-6):184–193.
45. Wohlgemuth S, et al. (2005) Recognizing and defining true Ras binding domains I: Biochemical analysis. *J Mol Biol* 348(3):741–758.
46. Pacold ME, et al. (2000) Crystal structure and functional analysis of Ras binding to its effector phosphoinositide 3-kinase gamma. *Cell* 103(6):931–943.
47. Eichinger L, et al. (2005) The genome of the social amoeba Dictyostelium discoideum. *Nature* 435(7038):43–57.
48. Robbins SM, Williams JG, Jermyn KA, Spiegelman GB, Weeks G (1989) Growing and developing Dictyostelium cells express different ras genes. *Proc Natl Acad Sci USA* 86(3):938–942.
49. Kae H, Lim CJ, Spiegelman GB, Weeks G (2004) Chemoattractant-induced Ras activation during Dictyostelium aggregation. *EMBO Rep* 5(6):602–606.
50. Ohashi K, Kiuchi T, Shoji K, Sampei K, Mizuno K (2012) Visualization of cofilin-actin and Ras-Raf interactions by bimolecular fluorescence complementation assays using a new pair of split Venus fragments. *Biotechniques* 52(1):45–50.
51. Iizuka R, Yamagishi-Shirasaki M, Funatsu T (2011) Kinetic study of de novo chromophore maturation of fluorescent proteins. *Anal Biochem* 414(2):173–178.
52. Seastone DJ, et al. (2001) The WASp-like protein scar regulates macropinocytosis, phagocytosis and endosomal membrane flow in Dictyostelium. *J Cell Sci* 114(Pt 14): 2673–2683.
53. Steffen A, et al. (2006) Filopodia formation in the absence of functional WAVE- and Arp2/3-complexes. *Mol Biol Cell* 17(6):2581–2591.
54. Innocenti M, et al. (2005) Abi1 regulates the activity of N-WASP and WAVE in distinct actin-based processes. *Nat Cell Biol* 7(10):969–976.
55. Brandt DT, et al. (2007) Dia1 and IQGAP1 interact in cell migration and phagocytic cup formation. *J Cell Biol* 178(2):193–200.
56. Naj X, Hoffmann AK, Himmel M, Linder S (2013) The formins FMNL1 and mDia1 regulate coiling phagocytosis of *Borrelia burgdorferi* by primary human macrophages. *Infect Immun* 81(5):1683–1695.
57. Hoffmann AK, Naj X, Linder S (2014) Daam1 is a regulator of filopodia formation and phagocytic uptake of *Borrelia burgdorferi* by primary human macrophages. *FASEB J* 28(7):3075–3089.
58. Hacker U, Albrecht R, Maniak M (1997) Fluid-phase uptake by macropinocytosis in Dictyostelium. *J Cell Sci* 110(Pt 2):105–112.
59. Romero S, et al. (2004) Formin is a processive motor that requires profilin to accelerate actin assembly and associated ATP hydrolysis. *Cell* 119(3):419–429.
60. Block J, et al. (2012) FMNL2 drives actin-based protrusion and migration downstream of Cdc42. *Curr Biol* 22(11):1005–1012.
61. Loisel TP, Boujemaa R, Pantaloni D, Carlier MF (1999) Reconstitution of actin-based motility of *Listeria* and *Shigella* using pure proteins. *Nature* 401(6753):613–616.
62. Chattwood A, Bolourani P, Weeks G (2014) RasG signaling is important for optimal folate chemotaxis in Dictyostelium. *BMC Cell Biol* 15:13.
63. Kölsch V, Charest PG, Firtel RA (2008) The regulation of cell motility and chemotaxis by phospholipid signaling. *J Cell Sci* 121(Pt 5):551–559.
64. Devreotes P, Horwitz AR (2015) Signaling networks that regulate cell migration. *Cold Spring Harb Perspect Biol* 7(8):a005959.
65. Tuxworth RI, et al. (1997) Dictyostelium RasG is required for normal motility and cytokinesis, but not growth. *J Cell Biol* 138(3):605–614.
66. Dames SA, et al. (2011) Structure, dynamics, lipid binding, and physiological relevance of the putative GTPase-binding domain of Dictyostelium formin C. *J Biol Chem* 286(42):36907–36920.
67. Takeya R, Taniguchi K, Narumiya S, Sumimoto H (2008) The mammalian formin FHOD1 is activated through phosphorylation by ROCK and mediates thrombin-induced stress fibre formation in endothelial cells. *EMBO J* 27(4):618–628.
68. Schulte A, et al. (2008) The human formin FHOD1 contains a bipartite structure of FH3 and GTPase-binding domains required for activation. *Structure* 16(9):1313–1323.
69. Dumontier M, Höcht P, Mintert U, Faix J (2000) Rac1 GTPases control filopodia formation, cell motility, endocytosis, cytokinesis and development in Dictyostelium. *J Cell Sci* 113(Pt 1):2253–2265.
70. Filić V, Marinović M, Faix J, Weber I (2012) A dual role for Rac1 GTPases in the regulation of cell motility. *J Cell Sci* 125(Pt 2):387–398.
71. Veltman DM, Akar G, Bosgraaf L, Van Haastert PJM (2009) A new set of small, extrachromosomal expression vectors for Dictyostelium discoideum. *Plasmid* 61(2): 110–118.
72. Schneider N, et al. (2003) A Lim protein involved in the progression of cytokinesis and regulation of the mitotic spindle. *Cell Motil Cytoskeleton* 56(2):130–139.
73. Faix J, Kreppel L, Shaulsky G, Schleicher M, Kimmel AR (2004) A rapid and efficient method to generate multiple gene disruptions in Dictyostelium discoideum using a single selectable marker and the Cre-loxP system. *Nucleic Acids Res* 32(19):e143.
74. Fey P, Dodson RJ, Basu S, Chisholm RL (2013) One stop shop for everything Dictyostelium: DictyBase and the Dicty Stock Center in 2012. *Methods Mol Biol* 983:59–92.
75. Breitsprecher D, et al. (2008) Clustering of VASP actively drives processive, WH2 domain-mediated actin filament elongation. *EMBO J* 27(22):2943–2954.
76. Schirenbeck A, Bretschneider T, Arasada R, Schleicher M, Faix J (2005) The Diaphanous-related formin dDia2 is required for the formation and maintenance of filopodia. *Nat Cell Biol* 7(6):619–625.
77. Spudich JA, Watt S (1971) The regulation of rabbit skeletal muscle contraction. I. Biochemical studies of the interaction of the tropomyosin-troponin complex with actin and the proteolytic fragments of myosin. *J Biol Chem* 246(15):4866–4871.
78. Gregg JHJH, Krefft M, Haas-Kraus A, Williams KLKL (1982) Antigenic differences detected between prespore cells of *Dictyostelium discoideum* and *Dictyostelium mucoroides* using monoclonal antibodies. *Exp Cell Res* 142(1):229–233.
79. Bertholdt G, Stadler J, Bozzaro S, Fichtner B, Gerisch G (1985) Carbohydrate and other epitopes of the contact site A glycoprotein of Dictyostelium discoideum as characterized by monoclonal antibodies. *Cell Differ* 16(3):187–202.
80. Faix J, et al. (1996) Cortexillins, major determinants of cell shape and size, are actin-bundling proteins with a parallel coiled-coil tail. *Cell* 86(4):631–642.
81. Witke W, Schleicher M, Noegel AA (1992) Redundancy in the microfilament system: abnormal development of Dictyostelium cells lacking two F-actin cross-linking proteins. *Cell* 68(1):53–62.
82. Maselli A, Laevsky G, Knecht DA (2002) Kinetics of binding, uptake and degradation of live fluorescent (DsRed) bacteria by Dictyostelium discoideum. *Microbiology* 148(Pt 2):413–420.